29 June 1979, Volume 204, Number 4400 SCIENCE

Fast Ionic Transport in Solids

Crystalline solids with liquid-like ionic conductivities are revolutionizing solid-state electrochemistry

Gregory C. Farrington and Jacqueline L. Briant

Summary. The discovery of inorganic solids with ionic conductivities comparable to those of aqueous electrolytes has revolutionized solid-state electrochemistry. Sodium beta alumina, a Na^+ conductor, and Li_xTiS_2, an intercalation compound with simultaneous Li^+ and electronic conductivity, are two of the best and most versatile fast ionic conductors. A wide variety of cations can replace Na^+ in beta alumina and Li^+ in Li_xTiS_2 and change the properties of the materials. Sodium beta alumina and Li_xTiS_2 are currently used in the development of high-energy density batteries for electric vehicles and electrical utility load leveling. Current research in solid ionic conductors is exploring new intercalation compounds, solid polymer electrolytes, and alkali ion and proton transport in crystalline solids.

In 1967 Yao and Kummer (*1*) reported that the crystalline solid sodium beta alumina has a sodium ion conductivity at 25°C comparable to that of aqueous NaCl (0.1 molar). Their discovery stimulated a revolution in battery technology and kindled interest in the general phenomenon of fast ionic transport in solids. Solids with high ionic conductivities, such as $RbAg_4I_5$ (*2*, *3*), had been known previously. However, none had sodium beta alumina's combination of high sodium ion conductivity, low electronic conductivity, and chemical stability necessary for practical application in batteries. From the initial discovery of sodium beta alumina has grown a diverse, multidisciplinary investigation into the science and applications of solids with high ionic conductivities. Such compounds are often called superionic conductors (*4*).

In this article we briefly review the fundamental mechanisms of ionic migration in crystalline solids. We then discuss alkali ion and proton transport in two closely related fast ionic conductors, beta and beta″ alumina, and also the properties of TiS_2, which supports both ionic and electronic conductivity. Finally, we review several solid electrolyte applications currently being developed, including high-energy density batteries for electric vehicle and load leveling applications, novel chemical sensors, and miniature solid-state batteries and displays.

Gregory C. Farrington is a member of the research staff and Jacqueline L. Briant is a member of the associate staff of General Electric Research and Development Center, Schenectady, New York 12301.

Ionic Transport Mechanisms

Simple alkali salts, such as LiCl, KCl, and LiF, have long been known to have measurable ionic conductivities (*5*). Frenkel (*6*) and Schottky (*7*) developed the classic microscopic models showing how ionic hopping among vacant or interstitial lattice sites can result in long-range ionic migration in a rigid lattice (Fig. 1). Frenkel defects, ions promoted to interstitial sites from normal lattice positions, are found, for example, for cations in alkaline-earth halides. Schottky defects, anion-cation vacancy pairs, occur typically in alkali halides and alkaline-earth oxides. Both Frenkel and Schottky defects can arise from intrinsic and extrinsic sources. Intrinsic defects occur in thermodynamic equilibrium with the crystal lattice. The driving force for their creation is the lattice disorder produced. Extrinsic vacancies occur to compensate the charge of impurities of different valence. For example, Ca^{2+} substitution for Na^+ in NaCl must be accompanied by one additional Cl^- or a Na^+ vacancy. Often the number of defects is dominated by impurities at lower temperatures and intrinsic equilibrium at higher temperatures.

Ionic transport in crystals is described classically by the vacancy, interstitial, and interstitialcy models (Fig. 1). The vacancy mechanism involves the motion of a vacancy through a lattice by successive ion hops in the direction opposite to vacancy motion. In the interstitial model an ion moves through a series of interstitial sites. The interstitialcy mechanism involves cooperative motion in which a lattice ion hops to an interstitial site and an interstitial ion fills the remaining vacancy. An additional model often applied to proton transport is the Grotthuss model. According to this mechanism, a proton tunnels from a site associated with one Lewis base to a site associated with another. This transfer is followed by the rotation of one or both bases to allow the process to be repeated.

For all these mechanisms, ionic conductivity, σ, in crystals can usually be described by an Arrhenius equation

$$\sigma = \frac{\sigma_0}{T} \exp(-E_A/kT)$$

in which σ_0 is a function of the ionic charge, concentration of mobile ions, and their attempt frequency and the jump distance; E_A is the activation energy for defect formation and motion; and k and T are the Boltzmann constant and temperature, respectively. Ionic conductivity is extremely sensitive to the value of E_A. In many materials, such as the alkali halides, conductivity falls into intrinsic and extrinsic temperature re-

0036-8075/79/0629-1371$02.00/0

gimes, depending on the dominant mechanism of defect formation (see curve for KCl in Fig. 2). Simple alkali halides have intrinsic activation energies between 1.2 and 2.2 electron volts; extrinsic activation energies vary between 0.4 and 1.5 eV. Their conductivities become appreciable, 10^{-4} to 10^{-3} $(ohm\text{-}cm)^{-1}$, only near their melting points, 600° to 900°C (*5*).

Ionic conductivity in solids covers a continuous spectrum of values. The solids $RbAg_4I_5$ (*2*) and sodium beta″ alumina (*8*) have the highest known ionic conductivities at 25°C, 2×10^{-1} $(ohm\text{-}cm)^{-1}$; values as low as 10^{-11} $(ohm\text{-}cm)^{-1}$ have been measured for H_3O^+ beta alumina (*9*). For comparison, the conductivity of 0.1*M* NaCl in water is 1.1×10^{-2} $(ohm\text{-}cm)^{-1}$ and the electronic conductivity of copper is 6×10^5 $(ohm\text{-}cm)^{-1}$ at 25°C.

For a solid to have high ionic conductivity at temperatures much lower than its melting point, it must have three characteristics: a high concentration of potential charge carriers, a high concentration of vacancies or interstitial sites, and a low activation energy for ion hopping from filled to unfilled sites. Crystal chemistry has identified many structures that meet the first two criteria, but the prediction of a low activation energy—essential for a compund to have high conductivity at 25° to 300°C—has been generally unsuccessful. The search for fast ionic conductors has proceeded by identifying structures that meet the first two criteria and by experimentally assessing the third.

Crystalline solids in which fast ionic conductivity is observed include stoichiometric compounds, such as AgI (*5*) and $RbAg_4I_5$, and nonstoichiometric compounds, such as sodium beta alumina. Some compounds, like Li_xTiS_2, support both ionic and electronic conductivity. Ionic motion can take place in one, two, or three dimensions, depending on crystal structure. One-dimensional ionic conductivity is found in compounds such as $LiAlSiO_4$ (beta eucryptite), which has a hexagonal structure in which lithium ions are found in channels parallel to the *c* axis (*10*). However, one-dimensional ionic motion can be easily blocked by a small concentration of crystal imperfections or impurities. Two-dimensional conductivity occurs in compounds that crystallize in layer structures, as do many oxides and sulfides. Examples include sodium beta alumina and Li_xTiS_2 (*11*). Three-dimensional conductivity is observed in the simple compound Li_3N (*12*) as well as in complex structures of interlocking polyhedra such as $Na_3Zr_2PSi_2O_{12}$ (*13*). Figure 2 summarizes the properties of a number of fast ionic conductors (*2, 8, 10, 12–18*).

In this article we have chosen to discuss the properties and applications of the alkali and protonic beta and beta″ aluminas and also of TiS_2. Among fast ionic conductors, beta alumina remains one of the best and most versatile. Its structure is host to many cations, including Li^+, K^+, Ag^+, Tl^+, Rb^+ (*1*), and NO^+ (*19*) as well as H^+ (*20*), $H(H_2O)_x^+$ (*21*), and NH_4^+ (*20*). Divalent ions such as Ca^{2+} and Ba^{2+} also replace sodium in beta alumina (*22*). The beta alumina isomorphs illustrate how structure and conductivity change as different ions are substituted in a common framework. Like beta alumina, TiS_2 accommodates a variety of guest species intercalated into its structure. It is an excellent example of a solid-state ionic-electronic conductor. Both sodium beta alumina and TiS_2 are close to commercial application. Readers interested in more extensive or more specific reviews of solid electrolytes may consult several recent publications (*23–25*).

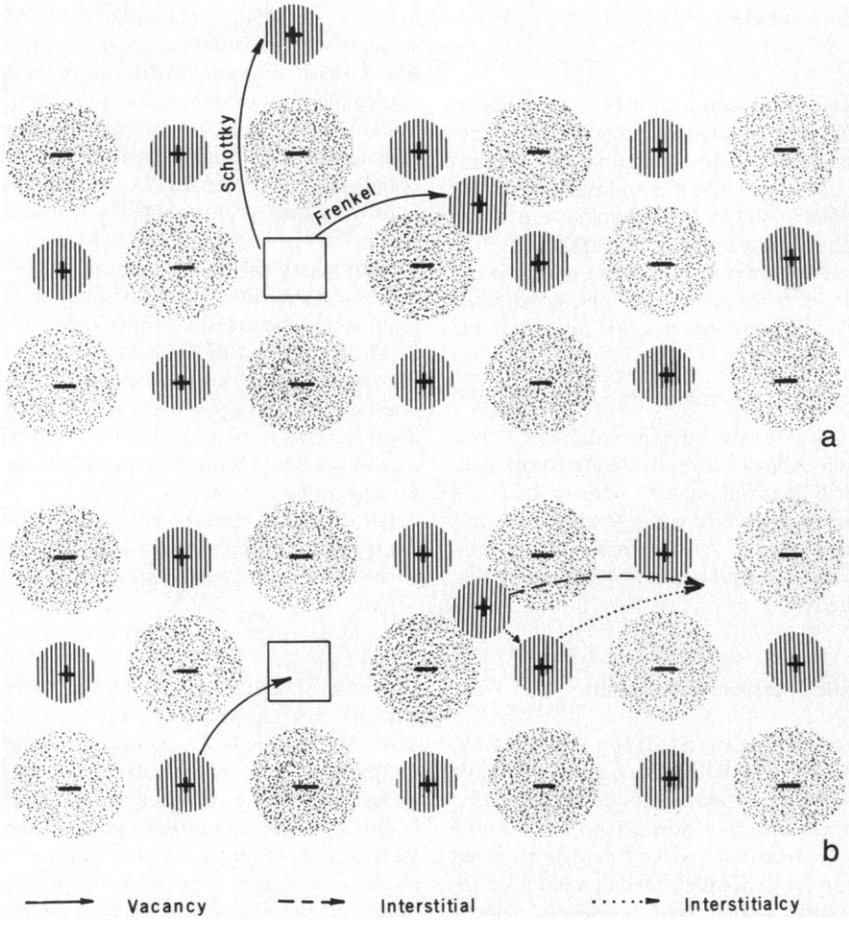

Fig. 1. (a) Frenkel (interstitial) and Schottky (vacancy) models of lattice defects that can result in ionic conductivity. (b) Three classical mechanisms for ionic conductivity in crystalline solids.

Sodium Beta and Beta″ Alumina

Sodium beta alumina is a nonstoichiometric compound of the general formula $(1+x)Na_2O{\cdot}11Al_2O_3$. It was first reported in 1916 by Rankin and Merwin (*26*), who, failing to detect the Na_2O content, considered it a modification of Al_2O_3. The misnomer has persisted despite later demonstration that it is a nonstoichiometric sodium aluminate containing excess Na_2O over the 1:11 composition (*1, 27, 28*). Yamaguchi (*29*) first reported a variant of sodium beta alumina with the general formula $Na_2O{\cdot}5Al_2O_3$ and designated it as sodium beta″ alumina. In Western literature, Thery and Briancon (*30, 31*) first discussed sodium beta″ alumina in 1962. Sodium beta″ alumina is generally synthesized as a ternary oxide in which MgO or Li_2O is added to stabilize the structure. We first discuss sodium beta and beta″ alumina, then the alkali and silver isomorphs, and finally the protonic forms. For each compound, we review composition, structure, and conductivity. We attempt to show how the properties of

the isomorphs vary as the size and chemical nature of the substituting ion change. Since the chemistry of the proton forms is extreme, it is discussed separately.

Both beta and beta″ alumina contain excess sodium beyond the ideal formula $Na_2O{\cdot}11Al_2O_3$ or $NaAl_{11}O_{17}$. According to the most widely accepted evidence (*32*), the general formula of beta alumina is $Na_{1+x}Al_{11}O_{17+x/2}$. The range of x is undetermined. Values up to 0.3 in single crystals have been reported (*27*). A typical composition is $1.24Na_2O{\cdot}11Al_2O_3$. The excess sodium ions are compensated by oxygen ions, which occupy specific interstitial sites in the crystal structure. In beta″ alumina, Mg^{2+} (or Li^+) substitutes for specific Al atoms in framework sites. To maintain charge neutrality, one additional sodium ion enters the structure for each Mg^{2+}; the general formula is $Na_{1+x}Mg_xAl_{11-x}O_{17}$. The full range for x in beta″ alumina is not known; a typical value is 0.67, which corresponds to a composition of $0.84Na_2O{\cdot}0.67MgO{\cdot}5.2Al_2O_3$.

Beta and beta″ alumina crystallize in layered structures (Fig. 3) (*27, 33, 34*). The sodium ions are found in relatively open conduction planes, which alternate with close-packed Al-O spinel-type blocks, named for their correspondence to the spinel ($MgAl_2O_4$) structure. Sodium ions can diffuse rapidly in two dimensions within the conduction planes. Each conduction plane is bounded by two close-packed layers of oxygen atoms held apart by Al-O-Al columns. The centers of the column oxygens define the conduction plane, a term that also refers to the entire region between the close-packed oxygen layers.

One critical difference between beta and beta″ alumina that influences ionic conductivity is the structural relationship of the two close-packed oxygen layers (Fig. 4). In beta alumina, the layers are superposed and the conduction plane is a mirror plane. In beta″ alumina, the spinel blocks are rotated 120° with respect to each other, the close-packed oxygen layers are staggered, and the conduction plane is not a mirror plane. The result is that beta″ alumina is a roomier structure for ionic motion.

One additional difference between the structures of the conducting planes in beta and beta″ alumina is the presence in beta alumina of interstitial oxygen ions locked in site 2 by aluminum ions in Frenkel defect sites. The discovery of the Frenkel defect by Roth *et al.* (*32*) provided convincing evidence that interstitial oxygens are the primary mechanism of charge compensation for the nonstoichiometric excess sodium in beta alumina. Charge compensation in beta″ alumina occurs by Mg^{2+} substitution for Al^{3+} in one of four tetrahedral aluminum sites in the spinel block. This substitution stabilizes the structure by relieving local strain.

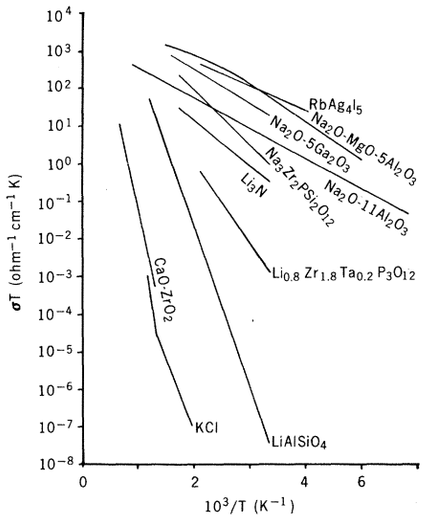

Fig. 2. Conductivities of various fast ionic conductors. For each compound except $CaO{\cdot}ZrO_2$ (O^{2-}) and $RbAg_4I_5$ (Ag^+), the mobile ion is the first element in the formula. Formulas in parentheses represent the particular compositions measured for materials having a range of compositions. References: $RbAg_4I_5$ (*2*); $Na_2O{\cdot}MgO{\cdot}5Al_2O_3$ (0.84 $Na_2O{\cdot}$ 0.67 $MgO{\cdot}5.2$ Al_2O_3) (*8*); $Na_2O{\cdot}5Ga_2O_3$ (1.14 $Na_2O{\cdot}5$ Ga_2O_3) (*14*); $Na_2O{\cdot}11Al_2O_3$ (1.16 $Na_2O{\cdot}11$ Al_2O_3) (*15*); $Na_3Zr_2PSi_2O_{12}$ (*13*); Li_3N (*12*); $Li_{0.8}Zr_{1.8}Ta_{0.2}P_3O_{12}$ (*16*); $LiAlSiO_4$ (*10*); $CaO{\cdot}ZrO_2$ (0.151 $CaO{\cdot}0.849$ ZrO_2) (*17*); and KCl (*18*).

Three crystallographically distinct sites are available for mobile ion occupation in beta alumina. They are given the names Beevers-Ross (BR or 1), mid-oxygen (mO or 2), and anti-Beevers-Ross (aBR or 3). The most favored site for sodium occupation is BR; the least favored aBR (*27, 32*). In stoichiometric beta alumina, one sodium ion would occupy each BR site. Excess sodium occurs as mO-mO split interstitial pairs. At high temperatures the differences in site energies become less significant, and the sodium density is distributed almost evenly along the hexagonal pathways. In $1.24Na_2O{\cdot}11Al_2O_3$, 38 percent of the total of sites 1 and 3 are vacant. Ionic diffusion takes place by zigzag ion hopping around the column oxygens. Sodium ions move along the plane defined by the centers of the column oxygens. The smallest gap for ion motion is in the aBR site, in which a sodium ion must move between two oxygen ions, one directly above and one directly below. This gap between the oxygen ions is 2.0 angstroms, sufficient for sodium ion (1.94 Å in diameter) but somewhat small for larger ions.

Beta″ alumina has three ion sites corresponding to those in beta alumina. However, sites 1 and 3 are equivalent, although inverted with respect to each other, and are referred to as BR-type sites. These sites have equal occupational probabilities and contain all of the sodium ions. In $0.84Na_2O{\cdot}0.67MgO{\cdot}$ $5.2Al_2O_3$, 17 percent of the BR-type sites are vacant. Sodium ion motion is undulatory with equilibrium positions 0.17 Å above the plane in site 1 and 0.17 Å below the plane in site 3. An important feature of the beta″ alumina structure is that the smallest gap for ion motion is not 2.0 Å as in site 3 of beta alumina, but 3.0 Å in site 2, where an ion moves between two column oxygens. As a result, ions larger than sodium are more mobile in beta″ alumina.

Sodium ion conductivity in beta and beta″ alumina single crystals is exceptionally high. Values for sodium beta alumina at 25°C vary from 0.030 (ohm-cm)$^{-1}$ (*35*) to 0.014 (ohm-cm)$^{-1}$ (*15*), depending on the method of crystal growth. For sodium beta″ alumina, single-crystal conductivities as high as 0.18 and as low as 0.014 (ohm-cm)$^{-1}$ (*8, 20*) have been measured at 25°C, again depending on the method of crystal growth. The activation energy for conductivity in sodium beta alumina is constant over an extraordinarily wide temperature range, at least −150° to 820°C (*15*). Specific values of activation energy range from 0.158 to 0.165 eV. For sodium beta″ alumina considerable variation is observed in the Arrhenius plots of crystals grown under slightly different conditions. In every case the activation energy decreases with increasing temperature (*8, 20*). The curvature may result from crystalline defects, which alter the microscopic diffusion pathway or the concentration of charge carriers as a function of temperature. Because ionic diffusion in both structures is defect-controlled, neither has a unique conductivity or activation energy. Both will vary with stoichiometry and the arrangement of defects. No detailed investigation of the influence of stoichiometry on conductivity in single crystals of either structure has appeared, although the variation of conductivity with stoichiometry in polycrystalline samples has been studied (*36*).

Wang *et al.* (*37*) have presented one of the most successful theoretical treatments of ionic motion in beta alumina. They found that the energy barrier for sodium ion hopping from a filled BR site to a vacant aBR site is about 2.7 eV. However, the energy barrier for motion

of one sodium from a mO-mO interstitial pair through the aBR site is lowered to 0.26 eV, close to the range of activation energies measured. They conclude that conductivity in sodium beta alumina occurs by a low-energy interstitialcy mechanism, as suggested by Whittingham and Huggins (*15*). This implies that sodium ions in stoichiometric beta alumina would be trapped in deep potential wells at BR sites and ionic diffusion would be very slow. No comparable calculations have appeared for sodium beta″ alumina, in which conductivity presumably occurs by a vacancy diffusion mechanism. The activated step is passage across the relatively low (less than 0.2 eV) potential barrier in the mO site.

Alkali and Silver Beta and Beta″ Aluminas

In this section we discuss how the properties of beta and beta″ alumina change when sodium is replaced by other alkali ions or silver. The patterns illustrate how ion size, ionic bonding within the conduction plane, and intercalated water influence fast ion motion. We first examine structure and conductivity in the beta alumina isomorphs, then in the beta″ isomorphs.

The simplest change that occurs in both beta and beta″ alumina on ion exchange is a slight swelling or contraction of the distance between the close-packed oxygen layers bounding the conduction plane (*1*). When sodium is replaced by larger alkali ions, the interplanar spacing increases. If the Al-O-Al bridging bonds did not constrain the movement of the oxygen layers, lithium exchange would be expected to decrease the spacing. But the oxygen layers cannot move close enough for Li^+ to sit in the middle of the plane and bond to each layer simultaneously. The Li^+ is deflected about 1 Å toward either of the close-packed layers, which move apart because of weakened interlayer bonding (*38*). The Ag^+ ion, although slightly larger than Na^+, causes a small contraction of the lattice.

Wide variation in the ionic distribution in the conduction plane as a function of ion type is seen in beta alumina. Even more than sodium ions at 25°C, potassium (*39*) and rubidium (*40*) ions predominantly occupy the BR sites, rather than the mO and aBR sites, as is consistent with their larger sizes. Silver ions preferentially occupy the BR site (*41*), although significant occupation of the aBR site occurs. Lithium positions have not been determined for pure lithium beta alumina, but in 1:1 Li-Na beta alumina, the lithium ions are in the mO sites deflected toward either oxygen plane, as previously noted, and the sodium ions are found primarily in the BR sites (*38*). All ions distribute more evenly in the conduction plane with increasing temperature.

The conductivities of the beta alumina isomorphs depend largely on E_A, since the preexponential factors (σ_0) are nearly equal (Table 1). An ion's size and tendency to bond to oxygen atoms in the conduction plane greatly affect its activation energy: E_A increases with increasing ionic size from Na^+ to Rb^+, as passage through the small aBR site requires increasing energy. The activation energy for Li^+ conductivity is higher than for sodium because of the extra energy required to overcome its off-plane bonding. Divalent ions, such as Ca^{2+} and Ba^{2+}, probably have very high activation energies for diffusion in beta alumina (*1*) as the result of strong local bond formation with the lattice. The activation energies for Na^+, K^+, Ag^+, and Rb^+ motion are constant over wide ranges of temperature, but the Arrhenius plot for Li^+ transport has been reported to have several distinct regions of differing slopes (*42*). Whether this is intrinsic to lithium motion or reflects more complex ion interaction within the conduction plane is not yet known.

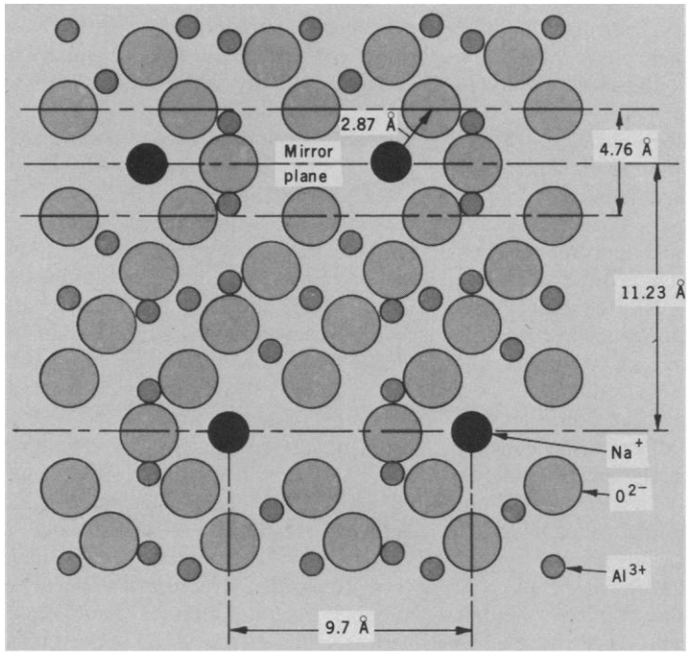

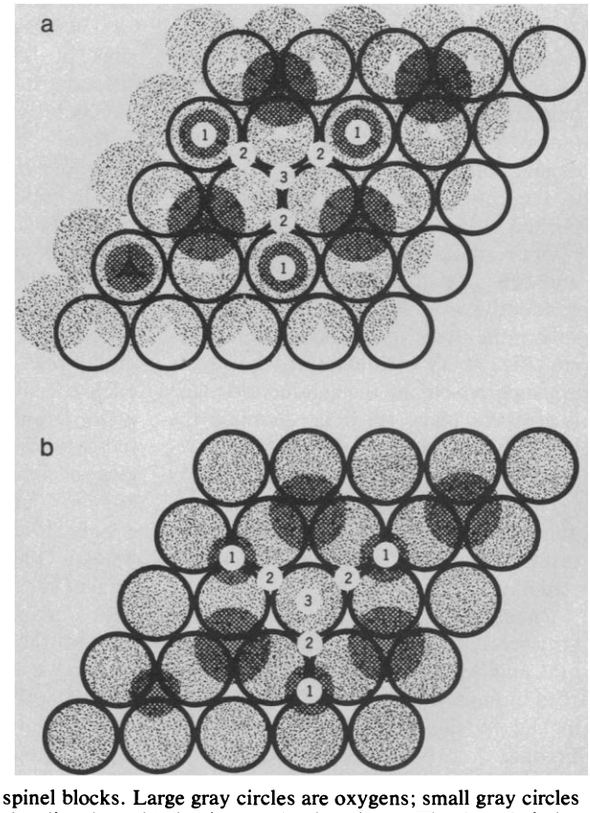

Fig. 3 (left). Beta alumina structure showing alternating conduction planes and spinel blocks. Large gray circles are oxygens; small gray circles are aluminums; black circles are sodiums. Fig. 4 (right). Sodium beta″ (a) and sodium beta (b) alumina conduction planes. The dotted circles are oxygens in the lower close-packed plane, the open circles are oxygens in the upper close-packed plane, and the crosshatched circles are column oxygens within the conduction plane. The smaller crosshatched circles are sodium ions, which diffuse along a zigzag 1-2-3-2-1 pathway.

Relatively little is known about the properties of the beta″ alumina isomorphs. X-ray data show that the interplanar spacing increases on K^+ exchange but decreases for Ag^+, as in beta alumina (*8*). However, detailed structures have not been determined for isomorphs other than sodium (*43*) and potassium (*44*). Single-crystal conductivities of K^+ and Ag^+ beta″ alumina have been measured. The conductivity of potassium beta″ alumina is comparable to that of sodium beta″ alumina (Table 2) and is more than 100 times greater than that of potassium beta alumina at 25°C (*8*). This qualitatively agrees with the prediction that ions larger than sodium will diffuse more rapidly in beta″ alumina than in beta alumina. The significantly lower conductivity of silver ions (*8*) compared to sodium and potassium must result from a decrease in the preexponential factor, perhaps reflecting different site occupation. The activation energies for sodium, potassium, and silver beta″ alumina all decrease with increasing temperature (*8*). An understanding of these observations awaits further investigation.

Finally, water can intercalate into the conduction plane of these beta and beta″ alumina isomorphs (*20, 45*). The extent of hydration increases from sodium to lithium beta alumina (*20, 45*). In hydrogen beta alumina, the extreme of the alkali series, water plays an essential role in conductivity, as will be discussed below. Potassium, silver, and rubidium beta alumina appear to absorb no water at all (*20, 45*). The alkali beta″ aluminas absorb more water than the corresponding beta aluminas (*45*). The water content of sodium forms is desorbed around 200°C. Nuclear-magnetic-resonance (NMR) data show that water in sodium beta alumina is present as relatively fixed molecules that do not undergo rapid translation or proton exchange even at 150°C (*46*). Intercalated water decreases the local motion and ionic conductivity in sodium beta alumina (*47*). Other small molecules, particularly those capable of hydrogen bonding to the oxygen framework, such as CH_3OH and H_2S, may also intercalate, although to our knowledge no one has reported such observations.

The preceding discussion illustrates that beta and beta″ alumina are not single compounds, but families having compositions with widely varying properties. General patterns of how the crystal chemistry determines ionic mobility in each structure are apparent. Sodium appears to have the optimum size for conduction in beta alumina. Ions larger or smaller have higher activation energies and lower conductivities. Larger ions tend to be more mobile in the beta″ alumina structure than in beta alumina. Ions with high charge-to-radius ratios tend to become trapped in local bonds with adjacent oxygens and hence have lower conductivities. The amount of intercalated water increases with decreasing ion size.

Table 1. Conductivity in beta alumina.

Ion	Radius (Å)	E_A (eV)	σ_0 (ohm-cm)$^{-1}$ K	σ(25°C) (ohm-cm)$^{-1}$	Temperature range (°C)	Reference
Li^+	0.68	0.19	5.4×10^1	1.3×10^{-4}	−100 to 180	(*42*)
		0.37	9.7×10^3	9.2×10^{-3}*	180 to 800	(*42*)
Na^+	0.98	0.16	2.5×10^3	1.4×10^{-2}	−150 to 820	(*15*)
Ag^+	1.26	0.17	1.6×10^3	6.7×10^{-3}	25 to 800	(*28*)
H_3O^+	1.32	0.78	8.1×10^4	1×10^{-11}	25 to 200	(*9*)
		1.3	5.9×10^3	9×10^{-11}*	250 to 500	(*9*)
K^+	1.33	0.30	1.5×10^3	6.5×10^{-5}	−70 to 820	(*42*)
Tl^+	1.47	0.36	6.8×10^2	2.2×10^{-6}	−20 to 800	(*42*)

*300°C.

Proton Conductors

We have reserved until this point a discussion of the protonic beta and beta″ aluminas, an intriguing and largely uninvestigated group of compounds in which sodium has been replaced by H^+, $H(H_2O)_x^+$, and NH_4^+. Several compositions show promise of fast proton conductivity; others are poor conductors. Although much less is known of their structures and properties, they are fascinating if only because fast proton conduction in inorganic solids is rare.

Many solids have measurable proton conductivities, but most are very low. Exceptions include H_3OClO_4 [10^{-4} (ohm-cm)$^{-1}$ at 25°C] (*48*) and newly discovered $HUO_2PO_4 \cdot 4H_2O$ [10^{-3} (ohm-cm)$^{-1}$ at 25°C] (*49*). Fast proton migration in each depends on a H_2O-H_3O^+ network through which protons diffuse by proton tunneling from one molecule to the next (Grotthuss mechanism). The transfer is followed by the rotation of one or both groups to allow it to continue. Therefore, fast proton transport in solids generally requires a closely linked network of donor/acceptor groups, such as the H_2O-H_3O^+ network. Few hydrated solids have high proton conductivities at elevated temperatures because dehydration destroys their conduction networks. $HUO_2PO_4 \cdot 4H_2O$ dehydrates to a poorly conducting phase somewhat above 80°C. Most other solid proton electrolytes (which have much lower conductivities at 25°C) dehydrate by about 100°C to compositions with conductivities less than 10^{-8} (ohm-cm)$^{-1}$.

The potential rewards of discovering a high-conductivity proton solid electrolyte are as enticing as the compounds are rare. A solid proton electrolyte with low electronic and high protonic conductivities between 100° and 400°C could have a major technological impact in new designs for fuel cells and water electrolyzers. No beta or beta″ alumina composition has yet been shown to have high proton conductivity from 100° to 400°C. However, NMR screening and initial conductivity measurements have suggested several that might (*50*). We do know that the protonic beta aluminas, while less stable than their alkali isomorphs, are far more stable than most hydrated inorganic proton electrolytes. The basic layer structure and substantial water content are retained to at least 750°C in the protonic beta aluminas (*21*) and at least 450°C in the beta″ aluminas (*50*). We present here brief summaries of what is currently known about the composition, structure, and conductivity of ammonium beta alumina, proton beta alumina, and hydronium beta and beta″ alumina.

One of the simplest protonic beta aluminas is ammonium beta alumina, $1.24(NH_4)_2O \cdot 11Al_2O_3$. Nuclear-magnetic-resonance data show that fast proton ex-

Table 2. Conductivity in beta″ alumina.

Ion	25°C			300°C			
	σ (ohm-cm)$^{-1}$	E_A (eV)	σ_0 (ohm-cm)$^{-1}$ K	σ (ohm-cm)$^{-1}$	E_A (eV)	σ_0 (ohm-cm)$^{-1}$ K	Reference
Na^+	1.8×10^{-1}	0.18	6.9×10^4	2.2	0.10	1.0×10^4	(*8*)
K^+	1.4×10^{-1}	0.18	3.9×10^4	5.3×10^{-1}	0.09	1.7×10^3	(*8*)
Ag^+	1.9×10^{-3}	0.22	3.3×10^3	3.2×10^{-2}	0.18	6.8×10^2	(*8*)

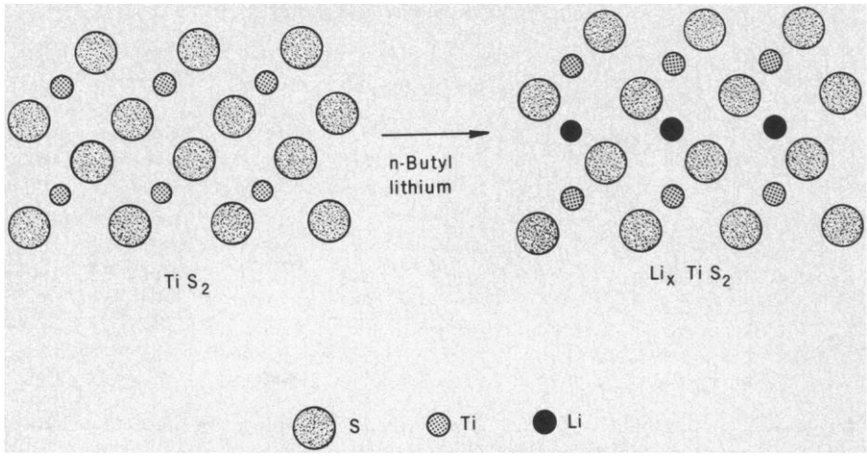

Fig. 5. Intercalation of Li^+ into TiS_2.

change within individual ammonium ions takes place even at −96°C. Above −10°C, evidence of longer-range proton or ammonium ion diffusion is seen (*46*). No evidence of fast proton conductivity is observed (*51*).

Between 425° and 475°C ammonium beta alumina dissociates into hydrogen beta alumina ($1.24H_2O{\cdot}11Al_2O_3$) and free ammonia, which diffuses out of the structure (*50*). Neutron diffraction data show that each resulting proton is bound to a column oxygen in one of six equivalent sites at 4.5 K (*52*). The NMR experiments have shown that protons are present as OH groups (*50*). According to both techniques, protons are disordered above about 150°C, although the conductivity is not greater than 10^{-5} (ohm-cm)$^{-1}$ at 300°C. Hydrogen beta alumina is stable until a partial and irreversible dehydration at 750°C.

When crystals of Monofrax sodium beta alumina are heated in concentrated sulfuric acid at 295°C for 2 to 3 weeks, the entire sodium content is replaced by protons and associated water (*21*). At 25°C the product corresponds to a hydronium (H_3O+) composition, $1.24(H_3O)_2O{\cdot}11Al_2O_3$ or $1.24H_2O{\cdot}11Al_2O_3{\cdot}2.5H_2O$(*53, 54*). Upon heating, a partial and reversible water loss occurs between 180° and 250°C, yielding $1.24H_2O{\cdot}11Al_2O_3{\cdot}1.2H_2O$. Complete decomposition takes place around 800°C (*21, 54*). Other compositions have been reported for hydronium beta alumina, perhaps reflecting differing starting materials and exchange techniques (*21, 55*). X-ray data, obtained on samples of uncertain composition, show an oxygen ion in each BR site deflected about 0.25 Å toward a neighboring column oxygen. The column oxygen is shifted about 0.35 Å toward the BR site, distorting the Al-O-Al angle from 180° to 157.6°C (*56*). A proton presumably forms a strong hydrogen bond between the two oxygens. The NMR data at −96°C on $1.24H_2O{\cdot}11Al_2O_3{\cdot}2.5H_2O$ are consistent with water molecules and more isolated protons in the planes, all of which rapidly exchange above 60°C. No water molecules are detected in the spectra of $1.24H_2O{\cdot}11Al_2O_3{\cdot}1.2H_2O$. All protons are in OH groups, tightly bound from −96° to 180°C (*50*).

The conductivity of $1.24H_2O{\cdot}Al_2O_3{\cdot}2.6H_2O$ is 10^{-10} to 10^{-11} (ohm-cm)$^{-1}$ at 25°C (*9*), 10^9 times smaller than that of sodium beta alumina. An even lower conductivity at 25°C is reported for $1.24H_2O{\cdot}11Al_2O_3{\cdot}1.3H_2O$ (*9*). Conductivity for these compositions increases with temperature with activation energies of 0.78 and 1.3 eV, respectively. Both activation energies are extremely high for beta alumina. They reflect strong hydrogen bonding in the conducting plane and result in low conductivities between 25° and 400°C.

Hydronium beta″ alumina is quite different (*50, 57*). The sodium content of sodium beta″ alumina can be replaced by protons and associated water molecules by exposure to aqueous acids, but the exact amount of water in the conducting plane is not well established. At least 1 and perhaps up to 1.7 water molecules per exchanged proton have been reported. The composition of hydronium beta″ alumina is $0.84H_2O{\cdot}0.67MgO{\cdot}5.2Al_2O_3{\cdot}xH_2O$ where $0 < x < 2.8$ (*50*). Like hydronium beta alumina, hydronium beta″ alumina undergoes a partial and reversible dehydration at 200° to 300°C. A second partial and irreversible dehydration occurs at 450°C. The crystal chemical bases of these dehydrations are not well understood.

We do know that ion transport, whether by H^+ or H_3O^+ motion, is more rapid in hydronium beta″ alumina than in hydronium beta alumina. At −96°C, the NMR spectra for hydronium beta and beta″ alumina are similar and consistent with water molecules and isolated protons in the planes. However, line narrowing, as the result of rapid proton exchange, occurs by −40°C in hydronium beta″ alumina, 100° lower than in hydronium beta alumina (*50*). Direct measurements find the conductivity of small crystals of hydronium beta″ alumina to be 10^{-5} to 10^{-7} (ohm-cm)$^{-1}$ at 25°C (*57, 58*).

Too little is known about hydronium beta″ alumina to understand why it behaves so differently from hydronium beta alumina. A key difference may be that an interconnected H_2O-H_3O^+-column O network can form in the beta″ alumina structure, providing a low-energy H^+ diffusion pathway. To create a close-packed H_2O-H_3O^+-column O network, each mO site must be filled with either H_2O or H_3O^+. The hydronium beta alumina composition that corresponds is $0.84H_2O{\cdot}0.67MgO{\cdot}5Al_2O_3{\cdot}2.8H_2O$, which is at the upper range of compositions reported. Investigations of both composition and conductivity in hydronium and also ammonium beta″ alumina are under way in an attempt to resolve these questions.

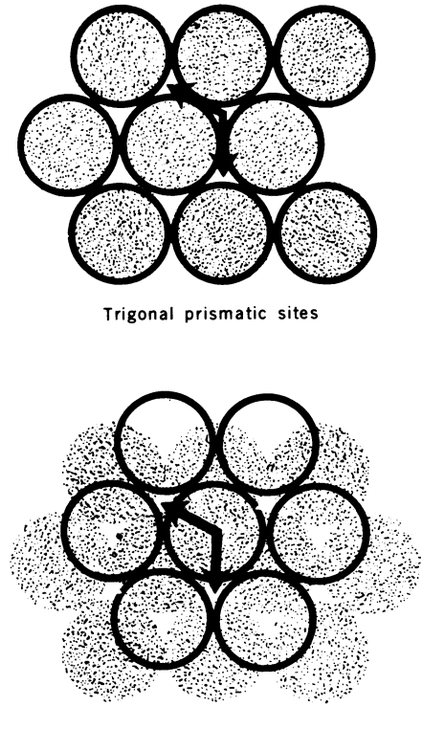

Fig. 6. Octahedral and tetrahedral coordination sites for intercalation ions in TiS_2. Diffusion pathways are shown by bold arrows. The dotted circles are sulfur atoms in the lower close-packed layer and the open circles are sulfur atoms in the upper layer.

Titanium Disulfide

Considerable interest in the field of fast ionic conductors at present is directed toward ionic electronic conductors, particularly intercalation compounds such as Li_xTiS_2. Titanium disulfide exemplifies a broad class of layered compounds with the general formula MX_2, in which M is a transition metal from groups IVB, VB, and VIB and X is a chalcogen such as S, Se, and Te (*59*). The compounds crystallize in layered structures, as shown in Fig. 5 for TiS_2. The transition metal atoms reside in octahedral or trigonal prismatic sites between two hexagonally close-packed chalcogen layers (Fig. 6). The MX_2 layers are held together by strong covalent bonds, but adjacent chalcogen layers are bound to each other only by weak van der Waals forces. A large variety of neutral guest molecules—Lewis bases such as NH_3, and pyridine—as well as cations such as Li^+, Na^+, and Ca^{2+} can intercalate between the weakly bound chalcogen layers of the host lattice. The ionic derivatives resemble beta alumina in that fast ionic motion takes place in the two-dimensional intercalation planes. Unlike beta alumina, the dichalcogenides are both ionic and electronic conductors with strongly anisotropic semiconducting or metallic electron transport in the MX_2 sandwiches.

Although intercalation compounds of graphite with halogens and alkali metals had been known for many years (*60*), Rudorff and Sick (*61*) and Rudorff (*62*) first reported the dichalcogenide intercalation compounds in 1959. Gamble *et al.* (*63*) later found them to be a new class of electronic superconductors. Broadhead and Trumbore (*64*) suggested them as host lattices for halogen "intercalation" for use in lithium battery cathodes. Whittingham (*11*) and Winn *et al.* (*65*) focused attention on Li_xTiS_2 as a fast Li^+ conductor that can function as an excellent lithium battery cathode. We will concentrate on discussing the properties of the disulfides, particularly Li_xTiS_2, and leave the broader class of compounds to more general reviews (*59*).

Different transition metals and different guest species alter the layer structure of the MS_2 compounds. When M is Mo or W, the close-packed sulfur layers of the MS_2 sandwich are superposed, and the transition metal occupies a trigonal prismatic site. With Ti, Zr, Hf, V, Cr, Re, Sn, Pb, and Pt the chalcogen layers are not superposed, and M is in an octahedral site. Separate disulfides with each symmetry are formed by Nb and Ta. Likewise, the intercalated species can occupy trigonal prismatic, tetrahedral, or octahedral sites, depending on the stacking of the MS_2 sandwiches.

During intercalation, the chalcogen layers move apart to accommodate the guest species, and the distance between the transition metal layers increases. No strong interlayer bonds, as found in beta alumina, constrain the movement of the MS_2 sandwiches with respect to each other. For a single cationic series, such as Li^+ to K^+, the Ti-Ti spacing increases linearly with ionic diameter (*59*). The Ti-Ti spacing is as large as 50 Å in $H_x(H_2O)_yTiS_2$ (*66*). The chalcogen layers also can easily slip along the weakly bonded van der Waals gap. Packing within the intercalated plane depends on stoichiometry and the nature of the guest species, and may even vary within a single composition and yield a poorly defined unit cell. The compound Li_xTiS_2 is a highly crystalline single phase for $0 < x < 1$ (*67*), in which Li^+ is found in octahedral sites (Fig. 6) (*59*). In contrast, Na_xTiS_2 forms several phases depending on the sodium content, and sodium ions are found in octahedral or trigonal prismatic sites (*68*).

The first preparation of Li_xTiS_2 was by reduction of TiS_2 in Li solutions in liquid NH_3 at $-40°$ to $-50°C$ (*61, 62*). During the reaction NH_3 intercalates with the Li^+, but it can be removed by gentle heating in vacuum. Alternate syntheses include reduction with *n*-butyllithium (Fig. 5) (*69*) and electrochemical reduction in the presence of lithium ions (*66*). Many neutral polar solvent molecules can simultaneously intercalate during reductive lithiation or by subsequent absorption to form a class of two-dimensional polyelectrolytes of the general formula $Li_xB_yTiS_2$ (*59, 70*). The stronger the electron donor properties of B, the greater its reactivity.

Although Li in Li_xTiS_2 is highly ionized, alkali metals in graphite intercalation compounds are not. The free energy of formation is large for Li_xTiS_2 (*67*) but small for the alkali-graphite compounds (*71*). Whereas Li_xTiS_2 behaves chemically as a lithium salt, the alkali-graphite compounds react similarly to the parent alkali metals. For example, C_8K reduces H_2O, but Li_xTiS_2 ($0 < x < 0.5$) forms stable cointercalates with water (*63*).

Little is known about the effect of cation type, stoichiometry, and the presence of cointercalated neutral molecules on the rate of ionic diffusion in M_xTiS_2. The simplest variable is the diffusion pathway—a network of trigonal prismatic sites if the chalcogen layers are superposed, or of alternating tetrahedral and octahedral sites if the layers are staggered (Fig. 6). In both structures there are twice as many ion sites as are filled in a 1:1 $MTiS_2$ composition. The compound $LiTiS_2$ crystallizes in an octahedral-tetrahedral array with a lithium ion in each octahedral site and the tetrahedral sites empty. Diffusion requires Li^+ hopping through the tetrahedral site, which is somewhat smaller than the octahedral site. The chemical diffusion coefficient of Li^+ in $LiTiS_2$ has been found to be very high, 10^{-8} square centimeters per second (25°C) (*72*), comparable to that of Li^+ in beta alumina. The compound Na_xTiS_2 crystallizes in the trigonal prismatic configuration for $0.4 < x < 0.6$ and the octahedral-tetrahedral configuration for $0.8 < x < 1.0$ (*61, 62*). The Na^+ diffusion coefficient is about 10^{-7} cm^2/sec (25°C) for $x = 0.42$ (*65*), but is much smaller in the octahedral-tetrahedral phase, perhaps reflecting a high activation energy for hopping through the constricted tetrahedral sites.

Cointercalated neutral molecules may have opposing effects on the rate of M^+ diffusion in $MTiS_2$. They may decrease the rate of diffusion by filling vacant ionic sites as well as increase the rate of diffusion by spreading apart the sulfur layers, increasing the size of the ionic sites, and shielding mobile ions from strong interactions with the sulfur layers. Nuclear-magnetic-resonance experiments show that both H_2O molecules and Na^+ ions are in rapid motion at 25°C in $Na_{0.3}(H_2O)_yTaS_2$. Lithium ions and H_2O in $Li_x(H_2O)_yTiS_2$ rapidly exchange with other ions and neutral Lewis bases if the H_2O is originally present as a cointercalate. Water diffusion into anhydrous $LiTiS_2$, in contrast, is very slow (*59*). In the absence of NH_3, which expands the van der Waals gap, the maximum composition of Na_xTiS_2 corresponds to $x = 0.8$, whereas a composition of $x = 1.0$ can be formed when NH_3 is present. All of these observations suggest that the decrease in activation energy as the result of spreading apart the sulfur layers (acting through the exponential term) increases the rate of ionic diffusion much more than potential blockage of diffusion pathways (affecting the preexponential term) decreases the rate of diffusion. The prediction from this, that pulling together the sulfur layers should decrease the ionic diffusion rate, is true. When TiS_2 is synthesized with a slight excess (6 percent) of Ti, the layered structure is retained and excess Ti atoms sit between the sulfur layers and hold them together; the Li^+ diffusion rate decreases dramatically (*59*).

Applications

Most applications of solid electrolytes are electrochemical: sensors, batteries, and solid-state displays. Here we discuss several devices that show promise of commercial realization.

A very simple application of solid electrolytes is in chemical sensors. If a membrane in which the ion, M, is mobile separates two chemical compositions with different activities of M, a potential is set up across the membrane that can be precisely related to the difference in the chemical activities. By fixing the activity on one side, an unknown activity on the other can be determined. In this way, the F^- conductor LaF_3 and its doped derivatives are used to make F^- ion-specific electrodes (*23*). Larger-scale application is envisioned for a novel O_2 sensor, which uses the O^{2-} conductor CaO + ZrO_2 (CSZ) in a Ni-NiO/CSZ/Pt sandwich in which the Ni/NiO fixes the oxygen activity on one side of the electrolyte (*73, 74*). Normally, oxygen sensors containing CSZ are sluggish in response at temperatures less than about 700°C because of low ionic conductivity in the membrane. However, by depositing CSZ films 10^3 to 10^4 Å thick, sensors are being developed with fast response at temperatures as low as 30° to 40°C. Thin-film CSZ sensors are currently being developed for automobile exhaust monitoring to optimize fuel consumption and minimize pollutant emission. Major problems are in producing reliable, long-lived, inexpensive sensors for use in a highly corrosive environment.

Of all the technologies that solid electrolytes may affect in the next decade, the most radical change may be in storage batteries. In any battery, two reactants, an oxidant and a reductant, each connected to an electronically conductive electrode, are separated by an ionically conductive, electronically insulating electrolyte. The object is to convert the free energy of the cell reaction, normally manifested as heat, into electrical energy. The cell is rechargeable if its initial chemical state can be readily restored by applying a reverse voltage and current. The electrolyte must be chemically inert to both cell reactants to avoid self-discharge. The stalwarts of conventional rechargeable batteries are the aqueous cells PbO_2/Pb, NiOOH/Cd, and NiOOH/Fe. Use of aqueous electrolytes restricts the design of new batteries to electrodes that will not react with water and eliminates many attractive candidates such as Li and Na. The amount of energy that can be stored in a given weight and volume in aqueous cells is therefore limited. Values of 40 to 60 watt-hours per kilogram and 0.3 and 0.6 watt-hour per cubic centimeter are typical for aqueous batteries.

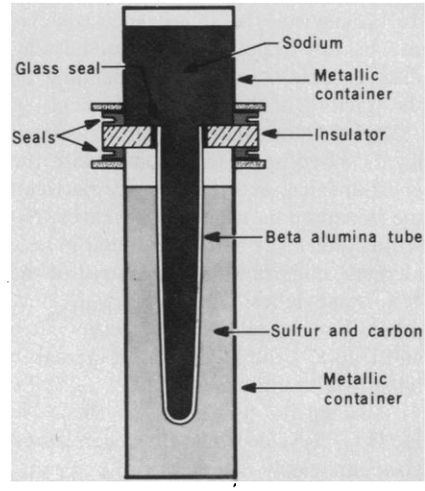

Fig. 7. Diagram of Na/Na^+ beta alumina/S electrochemical cell.

Batteries that could store two to three times as much energy per unit weight and volume as present aqueous cells and use less expensive reactants could make electric vehicle propulsion and off-peak electric power storage (load leveling) with batteries practicable. Replacement of aqueous electrolytes with more stable solid electrolytes, as in the Na/beta alumina/S cell, or organic liquid electrolytes, as in the Li/dioxolane/TiS_2 cell, are two approaches to developing high-energy density batteries.

The Na/beta alumina/S cell (Fig. 7) uses two liquid reactants, Na and S, separated by a polycrystalline membrane of beta alumina. Sodium beta alumina has all the properties necessary for an electrolyte membrane in the cell. It is chemically stable to sodium as well as to sulfur, ionically conductive, electronically insulating, and its composition does not change with sodium passage. The reactants, Na and S, are cheap and abundant.

To keep both Na and S molten, the Na/S cell operates between 300° and 350°C. During discharge, Na is oxidized to Na^+ at the Na/beta alumina interface. The Na^+ migrates through the beta alumina to the sulfur compartment. Concurrent sulfur reduction ultimately produces Na_2S_3 as the discharge product. The entire reaction sequence can be reversed by applying a reverse voltage and current.

Discovered initially in the Ford Laboratories, Na/S cells are in active development in Japan, Europe, and the United States. The goals of Na/S cells for load leveling are formidable: 10-year life and 200 cycles per year at 75 percent minimum energy efficiency. Practical cells of the same energy and power are four times lighter and two times smaller than Pb/PbO_2 cells. Current challenges are in developing simple and inexpensive technology for cell manufacture.

The Li/TiS_2 cells are another approach to high-density energy storage. They operate in a temperature range, 0° to 100°C, somewhat more appropriate for small consumer application and electric vehicle use. The use of TiS_2 is an elegant solution to the problems of the nonaqueous cell cathode. It has both electronic and ionic conductivity, a wide range of composition without phase change, relatively small volume change (10 percent) over the range of use, and it is a good oxidizing agent (*11, 75*). Laboratory Li/TiS_2 cells using a liquid electrolyte have achieved energy storage of 100 W-hour/kg at acceptable rates of discharge. The critical problem in any large-scale application of Li/TiS_2 cells is in long-term Li electrode stability. In a practical system, Li must be plated and stripped 10 to 100 times for small applications and 100 to 1000 times over the lifetime of an electric vehicle battery without sloughing off the electrode or reacting with the solvent. A lithium electrode/nonaqueous electrolyte combination satisfying these criteria has not yet been reported. Considerable efforts to solve the problems of lithium cycling are under way in many laboratories.

Finally, early in the development of fast ionic conductors, there was much enthusiasm for developing ionic analogs of solid-state electronic devices for memory and logic functions. Little of practical interest has come about, partly because electronic devices are so versatile, fast, and inexpensive. But two areas in which solid electrolytes might make unique contributions are in solid-state optical displays and miniature solid-state batteries.

Green and Kang (*76*) have exploited the electrochromic properties of $Na_x \times WO_3$, a compound that is blue in the Na_xWO_3 form and pale yellow as WO_3. By appropriate thin-film techniques, they prepared an all solid-state electrochromic display that can change color in a fraction of a second. Further development may produce a truly practical solid-state display.

In a similar technology, miniature solid-state batteries have been proposed (*77*) in which two solid ionic/electronic conductors with different activities of a common mobile ion, M, are separated by a solid ionic conductor of M. This solid-state analog of conventional batteries might be used for very low current (10^{-6}

to 10^{-9} ampere) applications, such as for memory retention in electronic circuitry. The concept is intriguing, but the problems of maintaining fast ion transfer across a solid/solid interface while one solid is changing composition are not trivial.

Current Research

The current challenges in the field of fast ionic conductors are in identifying and designing new fast ionic conductors and in understanding the nature of individual and collective ionic motion in solids. A major goal is to understand how a solid electrolyte's structure and its activation energy for ion motion are interrelated. These studies involve characterization of structure, ionic bonding, and ionic motion by neutron and x-ray diffraction, solid-state NMR, diffusion and conductivity measurements, and Raman and infrared spectroscopy, among other techniques. Stoichiometric compounds in which conductivity is intrinsic, such as AgI and $RbAg_4I_5$, are more easily understood than compounds that exist over ranges of composition. Beta and beta″ alumina are examples of the latter, nonstoichiometric compositions, in which extrinsic factors control ion motion. Specific topics being explored include the effect of ion-ion, or coionic, interactions on ionic distribution and conductivity in mixed Li^+-Na^+ beta alumina and Na^+-K^+ gallate. Recent reports discuss conductivity (*78, 79*), structure (*38*), and local ion motion and bonding in Li^+-Na^+ beta alumina (*80*) and conductivity in Na^+-K^+ gallate (*81*). Similar investigations are under way with TiS_2.

Of all the potential new solid electrolytes, the discovery of a compound with high H^+ or O^{2-} conductivity, low electronic conductivity, and excellent chemical stability from 100° to 400°C could have the greatest technological impact. With such a material, entirely new fuel cells and water electrolyzers might be designed that would make energy storage and transport in the form of hydrogen economical. Research characterizing and extending the temperature range of fast proton transport in $HOU_2PO_4 \cdot 4H_2O$ and its derivatives is under way. All of the protonic forms of beta and beta″ alumina are also being studied.

The study of intercalation compounds, stimulated by research on TiS_2, is active. One object is to identify compounds like TiS_2 that intercalate Li over a wide range of composition and simultaneously have fast ionic transport, high electronic conductivity, and a high free energy of reaction with Li. Such materials are in demand as electrodes in high-energy density lithium batteries.

An exciting new direction in fast ionic conductor research is in ionic conductivity in polymers. Armand *et al.* (*82*) recently found, for example, that polyethylene oxide–LiSCN complexes have conductivities greater than 10^{-5} $(ohm\text{-}cm)^{-1}$ above 40° to 80°C. The use of solid polymer ionic conductors, as both electrolytes and electrodes, may ultimately lead to successful all solid-state batteries. Understanding ionic motion in artificial polymers should also illuminate the mechanism of ionic conductivity in biochemical membranes.

References and Notes

1. Y-F. Y. Yao and J. T. Kummer, *J. Inorg. Nucl. Chem.* **29**, 2453 (1967).
2. B. B. Owens and G. R. Argue, *Science* **157**, 308 (1967).
3. J. B. Bradley and P. D. Greene, *Trans. Faraday Soc.* **63**, 424 (1967).
4. Use of this term should not imply an analogy to electronic superconductors.
5. R. F. Friauf, in *Physics of Electrolytes*, J. Hladik, Ed. (Academic Press, London, 1972), vol. 2, pp. 1112–1114.
6. J. Frenkel, *Z. Phys.* **35**, 652 (1926).
7. W. Schottky, *Z. Phys. Chem. Abt. B* **29**, 335 (1935).
8. J. L. Briant and G. C. Farrington, in preparation.
9. G. C. Farrington, J. L. Briant, M. W. Breiter, W. L. Roth, *J. Solid State Chem.* **24**, 311 (1978).
10. U. v. Alpen and H. Schulz, *Extended Abstr. Electrochem. Soc.* **77-2** (1977), abstract 17.
11. M. S. Whittingham, *Science* **192**, 1126 (1976).
12. U. v. Alpen and G. Muller, *Extended Abstr. Electrochem. Soc.* **77-2** (1977), abstract 19.
13. J. B. Goodenough, H. Y-P. Hong, J. A. Kafalas, *Mater. Res. Bull.* **11**, 203 (1976).
14. G. V. Chandrashekhar and L. M. Foster, *J. Electrochem. Soc.* **124**, 329 (1977).
15. M. S. Whittingham and R. A Huggins, *J. Chem. Phys.* **54**, 414 (1971).
16. R. D. Shannon, B. E. Taylor, A. D. English, T. Berzins, *Electrochim. Acta* **22**, 783 (1977).
17. F. Hund, *Z. Phys. Chem.* **199**, 142 (1952).
18. T. Miyata, R. Sano, T. Tomiki, *J. Phys. Soc. Jpn.* **20**, 638 (1965).
19. R. H. Radzilowski and J. T Kummer, *Inorg. Chem.* **8**, 2531 (1969).
20. J. T. Kummer, *Prog. Solid State Chem.* **7**, 141 (1972).
21. H. Saalfeld, H. Matthies, S. K. Datta, *Ber. Dtsch. Keram. Ges.* **45**, 212 (1968).
22. N. A. Toropov and M. M. Stukalova, *C. R. (Dokl.) Acad. Sci. URSS* **24**, 459 (1939).
23. A. Hooper, *Contemp. Phys.* **19**, 147 (1978).
24. J. H. Kennedy, in *Solid Electrolytes*, S. Geller, Ed. (Springer-Verlag, New York, 1977), p. 105.
25. P. Hagenmuller and W. van Gool, *Solid Electrolytes* (Academic Press, New York, 1978).
26. G. A. Rankin and H. E. Merwin, *J. Am. Chem. Soc.* **38**, 568 (1916).
27. C. R. Peters, M. Bettman, J. W. Moore, M. D. Glick, *Acta Crystallogr. Sect. B* **27**, 1826 (1971).
28. M. S. Whittingham and R. A. Huggins, *J. Electrochem. Soc.* **118**, 1 (1971).
29. G. Yamaguchi, *J. Electrochem. Soc. Jpn.* **11**, 260 (1943).
30. J. Thery and D. Briancon, *C. R. Acad. Sci* **254**, 2782 (1962).
31. ———, *Rev. Hautes Temp. Refrac.* **1**, 221 (1964).
32. W. L. Roth, F. Reidinger, S. LaPlaca, in *Superionic Conductors*, G. D. Mahan and W. L. Roth, Eds. (Plenum, New York, 1976), p. 223.
33. C. A. Beevers and M. A. Ross, *Z. Kristallogr.* **97**, 59 (1937).
34. W. L. Bragg, C. Gottfried, J. West, *ibid.* **77**, 255 (1931).
35. W. L. Fielder, H. E. Kautz, J. S. Fordyce, J. Singer, *J. Electrochem. Soc.* **122**, 528 (1975).
36. J. H. Kennedy and A. F. Sammells, *ibid.* **119**, 1609 (1972).
37. J. C. Wang, M. Gaffari, Sang-il Choi, *J. Chem. Phys.* **63**, 772 (1975).
38. B. C. Tofield and G. C. Farrington, *Nature (London)*, in press.
39. P. D. Dernier and J. P. Remeika, *J. Solid State Chem.* **17**, 245 (1976).
40. T. Kodama and G. Muto, *ibid.* **19**, 35 (1976).
41. W. L. Roth, *ibid.* **4**, 60 (1972).
42. M. S. Whittingham and R. A. Huggins, in *Solid State Chemistry*, R. S. Roth and S. J. Schneider, Jr., Eds. (Spec. Publ. 364, National Bureau of Standards, Washington, D.C., 1972), p. 148.
43. M. Bettman and C. R. Peters, *J. Phys. Chem.* **73**, 1774 (1969).
44. G. Yamaguchi and K. Suzuki, *Bull. Chem. Soc. Jpn.* **41**, 93 (1968).
45. G. C. Farrington, in *Membrane Transport Processes* (Raven, New York, 1979), vol. 3, p. 43.
46. H. S. Story, unpublished results.
47. D. Kline, H. S. Story, W. L. Roth, *J. Chem. Phys.* **57**, 5180 (1972).
48. A. Potier and D. Rousselet, *J. Chim. Phys.* **70**, 873 (1973).
49. M. G. Shilton and A. T. Howe, *Mater. Res. Bull.* **12**, 701 (1977).
50. G. C. Farrington, J. L. Briant, H. S. Story, W. C. Bailey, *Electrochim. Acta*, in press.
51. J. D. Axe, L. M. Corliss, J. M. Hastings, W. L. Roth, O. Muller, *J. Phys. Chem. Solids* **39**, 155 (1978).
52. W. A. England, A. J. Jacobson, B. C. Tofield, *J. Chem Soc. Chem. Commun.* (1976), p. 895.
53. M. W. Breiter, G. C. Farrington, W. L. Roth, J. L. Duffy, *Mater. Res. Bull.* **12**, 895 (1977).
54. W. L. Roth, M. W. Breiter, G. C. Farrington, *J. Solid State Chem.* **24**, 321 (1978).
55. P. Colomban, G. Lucazeau, R. Mercier, A. Novak, *J. Chem. Phys.* **67**, 5244 (1977).
56. V. K. Kato and H. Saalfeld, *Acta Crystallogr. Sect. B* **33**, 1596 (1977).
57. G. C. Farrington and J. L. Briant, *Mater. Res. Bull.* **13**, 763 (1978).
58. G. C. Farrington, unpublished results.
59. M. S. Whittingham, *Prog. Solid State Chem.* **12**, 41 (1978).
60. K. Fredenhagen and G. Cadenbach, *Z. Anorg. Allg. Chem.* **158**, 249 (1926).
61. W. Rudorff and H. H. Sick, *Angew. Chem.* **71**, 127 (1959).
62. W. Rudorff, *ibid.*, p. 487.
63. F. R. Gamble, J. H. Osiecki, M. Cais, R. Pisharody, F. J. DiSalvo, T. H. Geballe, *Science* **174**, 493 (1971).
64. J. Broadhead and F. A. Trumbore, *Extended Abstr. Electrochem. Soc.* **73-1** (1973), abstracts 178 and 179.
65. D. A. Winn, J. M. Schemilt, B. C. H. Steele, *Mater. Res. Bull.* **11**, 559 (1976).
66. M. S. Whittingham, *J. Chem. Soc. Chem. Commun.* (1974), p. 328.
67. ———, *J. Electrochem. Soc.* **123**, 315 (1976).
68. W. Rudorff, *Chimia* **19**, 489 (1965).
69. M. B. Dines, *Mater. Res. Bull.* **10**, 287 (1975).
70. R. Schollhorn, A. Lerf, F. Sernetz, *Z. Naturforsch. Teil B* **29**, 810 (1974).
71. S. Aronson, F. J. Salzano, B. Bellafiore, *J. Chem. Phys.* **49**, 434 (1968).
72. M. S. Whittingham, in *Electrode Materials and Processes for Energy Conversion and Storage*, J. D. E. McIntyre, S. Srinivason, F. G. Will, Eds. (Electrochemical Society, Princeton, N.J., 1977), p.784.
73. M. Croset, P. Schnell, G. Velasco, J. Siejka, *J. Appl. Phys.* **48**, 775 (1977).
74. J. P. Schnell, G. Velasco, M. Croset, J. Siejka, *Extended Abstr. Electrochem. Soc.* **78-1** (1978), abstract 100.
75. M. Lazzari, G. Razzini, B. Scrosati, *J. Power Sources* **1**, 57 (1976).
76. M. Green and K. S. Kang, *Thin Solid Films* **40**, L19 (1977).
77. G. J. Dudley and B. C. H. Steele, *J. Mater. Sci.* **13**, 1267 (1978).
78. W. L. Roth and G. C. Farrington, *Science* **196**, 1332 (1977).
79. G. C. Farrington and W. L. Roth, *Electrochim. Acta* **22**, 767 (1977).
80. R. R. Dubin and P. A. Casabella, *ibid.*, in press.
81. L. M. Foster and G. V. Chandrashekhar, *2nd Int. Meet. Solid Electrolytes*, St. Andrews, Scotland (September 1978), extended abstract 5.1.
82. M. Armand, J. M. Chabagno, M. Duclot, *2nd Int. Meet. Solid Electrolytes*, St. Andrews, Scotland (September 1978), extended abstract 6.5.1.